RESEARCH ARTICLE

3D-Printed β-Tricalcium Phosphate Scaffolds Promote Osteogenic Differentiation of Bone Marrow-Deprived Mesenchymal Stem Cells in an N6-methyladenosine-Dependent Manner

Xin Jiao[1†], Xin Sun[1†], Wentao Li[1†], Wenxiang Chu[2], Yuxin Zhang[3], Yiming Li[1], Zengguang Wang[1], Xianhao Zhou[1], Jie Ma[1], Chen Xu[1], Kerong Dai[1], Jinwu Wang[1*], Yaokai Gan[1*]

[1]Department of Orthopaedic Surgery, Shanghai Ninth People's Hospital, Shanghai JiaoTong University School of Medicine, No. 639 Zhi Zao Ju Road, Huangpu District, Shanghai, China
[2]Department of Orthopaedic Surgery, Changzheng Hospital, Naval Medical University, No. 415 Fengyang Road, Huangpu District, Shanghai, China
[3]Department of Rehabilitation Medicine, Shanghai Ninth People's Hospital, Shanghai JiaoTong University School of Medicine, No.639 Zhi Zao Ju Road, Huangpu District, Shanghai, China
[†]*These authors contribute equally to this work.*

Abstract: Bone defect is a serious orthopedic disease which has been studied for a long time. Alternative degradable biomaterials are required for bone repairing and regeneration to address the limitation of autogenous bone. β-tricalcium phosphate (β-TCP) is an alternative material with good cytocompatibility and has been used in bone defect treatment. However, whether β-TCP contributes to osteogenesis of bone marrow stem cells (BMSCs) through N6-methyladenosine (m6A) modification remains unknown. To address this issue, we verified the effects of β-TCP on osteogenesis of BMSCs. We also studied the expression of m6A-related enzymes in BMSCs after β-TCP treatment. Furthermore, the m6A level and stability of Runt-related transcription factor 2 (RUNX2) mRNA were investigated after β-TCP treatment. Finally, rat calvarial defect models were performed to detect expression level of osteogenic factors and m6A-related enzymes after the stimulation of three-dimension (3D)-printed β-TCP scaffolds. We found that β-TCP showed good biocompatibility and was osteoinductive. Meanwhile, methyltransferase-like 3 (METTL3) increased, causing the elevation of m6A level of RUNX2, results in stabler RUNX2 mRNA level. At last, based on the animal experiments, we demonstrated that the increase of RUNX2 and METTL3 levels was induced by β-TCP. These findings suggest that METTL3 increases the m6A level of RUNX2 mRNA after β-TCP induction, contributing to its stability, and the results in vivo also confirmed the osteogenic and bone-repair properties of β-TCP.

Keywords: β-tricalcium phosphate; Osteogenic differentiation; Bone marrow stem cells; Runt-related transcription factor 2; N6-methyladenosine

*Correspondence to: Jinwu Wang, Department of Orthopaedic Surgery, Shanghai Ninth People's Hospital, Shanghai JiaoTong University School of Medicine, No. 639 Zhi Zao Ju Road, Huangpu District, Shanghai, China; wangjw@sjtu.edu.cn; Yaokai Gan, Department of Orthopaedic Surgery, Shanghai Ninth People's Hospital, Shanghai JiaoTong University School of Medicine, No. 639 Zhi Zao Ju Road, Huangpu District, Shanghai, China; ganyk2004@126.com

Received: November 30, 2021; **Accepted:** February 5, 2022; **Published Online:** March 22, 2022

Citation: Jiao X, Sun X, Li W, *et al.,* 2022, 3D-Printed β-Tricalcium Phosphate Scaffolds Promote Osteogenic Differentiation of Bone Marrow-Deprived Mesenchymal Stem Cells in an N6-methyladenosine-Dependent Manner. *Int J Bioprint,* 8(2):544. http://doi.org/10.18063/ijb.v8i2.544

1. Introduction

Bone defect is one of the most common diseases encountered in the field of orthopedics. With the development of tissue engineering, allochthonous and autogenous bones have commonly been used for transplantation into the site of bone defects for therapeutic purposes[1]. However, this never addresses the problems, such as a shortage of bone sources and high infection rates. In view of the limitation of bone sources, degradable biomaterials such as hydroxyapatite (HA) and β-tricalcium phosphate (β-TCP) have become alternative choices for use in bone repair. β-TCP has been widely applied in clinical treatments due to their promising results. β-TCP has several beneficial properties in the aspects of biocompatibility, osteoconductivity, osteoinductivity, and biodegradability, and can be easily manufactured into porous structures, which further improves its biodegradability and makes it suitable as a bone substitute for clinical application. Numerous clinical trials have shown that β-TCP has a similar effect on bone repair as allografts[1]. Conventionally, β-TCP is used in the shape of disks or granules. Three-dimensional (3D) printing technology, as an emerging technology, has provided a new prospect in the treatment of bone defect. 3D printing can be used to make porous β-TCP, which is beneficial for ingrowth of new bone. In addition, β-TCP combined with bone marrow mesenchymal stem cells (bone marrow stem cells [BMSCs]) has shown significantly higher degree of new bone formation compared to β-TCP alone[2]. β-TCP/BMSCs combination could be used to treat bone defects, bone nonunion, and other orthopedic diseases requiring bone implantation, with a lower infection rate and a higher success rate of artificial bone implantation[3-7]. The osteoinductivity of β-TCP is probably related to the osteogenesis induced by BMSCs. It has been suggested that β-TCP promotes upregulation of osteocalcin (OCN), osteopontin (OPN), bone sialoprotein (BSP), and bone morphogenetic protein 2[8]. Moreover, Runt-related transcription factor 2 (RUNX2), the key transcription factor in osteogenesis of BMSCs, was also increased in expression level after 7 days of TCP stimulation[9]. However, the mechanism by which β-TCP contributes to the high expression of RUNX2 in BMSCs is not fully understood.

RUNX2 is an indispensable transcriptional factor for the commitment of mesenchymal stem cells toward the osteoblast lineage[10]. Knockout of RUNX2 causes osteogenesis blockage at the cartilage stage, suggesting that RUNX2 is a promoter of early mineralization[11]. Mechanistically, RUNX2, as a transcriptional factor, can activate a large number of bone-related genes, including OCN, OPN, bone sialoprotein, and alkaline phosphatase (ALP)[12]. The osteoblast differentiation program also requires the activation of the genes like osterix to encode a transcriptional factor downstream of RUNX2[13]. Notably, RUNX2 is also regulated by N6-methyladenosine (m6A) RNA methylation. Yan *et al*. discovered the dual signaling cascades of osteogenic pathways: (i) Methyltransferase-like 3 (METTL3) upregulates m6A methylation of RUNX2, which increases RUNX2 stability and level, and contributes to osteogenesis; and (ii) METTL3 increases m6A methylation of pre-miR-320, decreases miR-320 levels, upregulates RUNX2 levels, and improves osteogenesis[14]. The dual mechanism of m6A modification on osteogenic differentiation may be caused by high or low levels of m6A modification[15]. However, it is still unknown if the upregulation of RUNX2 after β-TCP stimulation is related to m6A modification.

M6A RNA methylation plays an important role in the regulation of numerous cell behaviors. M6A works through three mechanisms: (i) Writing, which is regulated by a methyltransferase complex consisting of METTL3, METTL14, Wilms tumor-1-associated protein (WTAP), and other methyltransferases, also known as writers[16-18]; (ii) erasing, which is regulated by demethylases fat mass and obesity-associated protein (FTO) and AlkB homolog 5 (ALKBH5), also known as erasers[19]; and (iii) reading, which is regulated by m6A-binding proteins, including YTH family proteins and IGF2BP family members, also known as readers. M6A also influences the osteogenic differentiation of BMSCs in different ways; however, there are contradictory opinions regarding the m6A regulation mechanism. Wu *et al*. found that parathyroid hormone (PTH)-induced osteogenic effects and the translation efficiency of parathyroid hormone receptor-1 (Pth1r) mRNA were decreased after the knockout of METTL3[20]. In contrast, METTL3 positively regulates myeloid differentiation primary response 88 (MYD88), activating the nuclear factor kappa B (NF-κB) signaling pathway, which is regarded as an inhibitor of osteogenesis. Meanwhile, the adverse effects of METTL3 can be reversed by ALKBH5[21]. M6A modification also regulates interaction between cell and extracellular matrix. For example, overexpression of METTL3 promotes accumulation of ECM in human Tenon's capsule fibroblasts[22]. However, the relationship between osteoinductivity of β-TCP and m6A modification remains unclear.

Therefore, the aim of this study is to prove that β-TCP might promote the osteogenesis of BMSCs by upregulating RUNX2 in an m6A-dependent manner, further providing new evidence to support the clinical use of β-TCP in bone defect treatment.

2. Materials and methods

2.1. 3D printing of β-TCP scaffolds

3D printing (REGENOVO, China) was utilized to make β-TCP scaffolds for implanting the β-TCP into Sprague-

Dawley (SD) rats. The β-TCP was mixed with Pluronic F-127 in an aqueous solution to obtain a β-TCP ink, and the mixture was then stirred until it was homogeneous. The ink was printed using a 22G needle, and the scaffolds were sintered at 1100°C for 3 h. The sintered β-TCP scaffolds were observed by scanning electron microscopy (SEM, USA). The scaffolds were then used for animal experiments.

2.2. Cell culture

Primary bone marrow mesenchymal stem cells were isolated after flushing the bone marrow of tibiae and femurs from 1-week-old SD rats. The BMSCs were cultured in α-minimum essential medium (α-MEM) (HyClone, SH30265.01, USA) supplemented with 10% fetal bovine serum (FBS; Gibco, 10099-141, USA), 1% penicillin/streptomycin (Gibco, 15140122, USA), and 0.4% gentamicin (Sangon Biotech, Shanghai, China), after which the cells were cultured at 37°C with 5% CO_2 and 95% humidity. The cell medium was changed every 3–4 days and the BMSCs were passaged when they were at nearly 80% confluence.

2.3. Preparation of β-TCP extract and characterization measurement of β-TCP extract

β-TCP powder was purchased from Kunshan Chinese Technology New Materials Co., Ltd (China). Two grams of the powder were incubated in 10 ml α-MEM at 37°C for 24 h to prepare β-TCP extract (200 mg/ml)[23-25]. Then, the mixture was centrifuged at 3000 ×g, and the supernatant was collected. The extract was sterilized through 0.22 μm filter membranes (Millipore, SLGPR33RB, USA) and stored at 4°C until further use. Size distribution and zeta potential were detected by Nano Sizer and Zeta potential Tester (Omni, USA). We diluted the β-TCP extract with α-MEM to concentrations of 1/32, 1/64, and 1/128. The concentrations of calcium (Ca) and phosphorus (P) ions in the three extracts with the concentrations of 1/32, 1/64, and 1/128 and α-MEM (control, ctrl) were detected using an inductively coupled plasma atomic emission spectrometer (ICP-AES; avio500, USA). The β-TCP extract at the three concentrations with α-MEM was used for cell experiments and supplemented with 10% FBS, 1% penicillin/streptomycin, 0.4% gentamicin, and osteogenic induction component (10 mM β-glycerophosphate, 50 μM ascorbic acid, and 10 nM dexamethasone). Cells in the control group were treated with α-MEM supplemented with 10% FBS, 1% penicillin/streptomycin, 0.4% gentamicin, and osteogenic induction component (10 mM β-glycerophosphate, 50 μM ascorbic acid, and 10 nM dexamethasone). The treatment lasted for 7 days.

2.4. Cytotoxicity assay

After being incubated in the above-mentioned extract with three replicates per group, BMSCs were seeded in 96-well plates at a density of 2.5×10^3 cells per well for cytotoxicity assay. Cell Counting Kit-8 (CCK-8) assay was performed on days 3 and 7 to assess the cytotoxicity of the β-TCP extract. The BMSCs were incubated in complete medium with 10% CCK-8 reagent (Dojindo, CK04-05, Japan) for 2 h at 37°C. The absorbance of the supernatant at 450 nm was measured using a microplate reader (Infinite M200 Pro, Tecan, Switzerland).

2.5. ALP staining

ALP staining was conducted on the BMSCs after incubation in the above extract for 7 days. BMSCs were washed 3 times with phosphate-buffered saline (PBS) and fixed with 4% paraformaldehyde (Beyotime, P0099, China) for 15 min. After that, the BMSCs were washed 3 times with PBS. An ALP kit (Hongqiao Lexiang, LRB-ALP, China) was used to perform ALP staining according to the manufacturer's instructions. The results were analyzed by ImageJ.

2.6. RNA extraction and quantitative real-time polymer chain reaction (PCR)

After a culture period of 7 days, the total RNA from the BMSCs seeded on 6-well plates, at a density of 2*10^5 cells per well, was extracted using TRIzol reagent (Invitrogen, 15596018, USA) following the manufacturer's instructions. The concentration of total RNA was measured using a NanoDrop ND-1000 Spectrophotometer (Thermo Fisher Scientific, USA), and 1000 ng of the extracted RNA was reverse transcribed to cDNA using PrimeScript Master Mix (TaKaRa, RR036A, Japan). For the qRT-PCR reaction, 2× SYBR Green qPCR Master Mix (Low ROX) (Bimake, B21703, China) and Applied Biosystems 7500 Real-Time PCR System (Applied Biosystems, Foster City, CA, USA) were used. Glyceraldehyde-3-phosphate dehydrogenase (GAPDH) was used as the quantitative control for normalization. The $2^{-\Delta\Delta Ct}$ method was used to calculate the relative mRNA levels. The primers used in this study are listed in **Table 1**.

2.7. Prediction of Runx2 m6A methylation sites

The prediction of possible sites modified by m6A was performed using SRAMP, a sequence-based m6A modification site predictor (www.cuilab.cn/sramp). The entire sequence of RUNX2 mRNA was imported onto the server. Then, the possible Runx2 m6A methylation sites were exported from the online tool automatically.

Table 1. Sequences of primers used in this study

Primer	Forward primer (5' to 3')	Reverse primer (5' to 3')
GAPDH	GGCAAGTTCAACGGCACAGT	GCCAGTAGACTCCACGACAT
METTL3	CAATGTGCAGCCCAACTGGATT	CACCATCTGGATACCTGTGCTT
WTAP	CTCGCCTCGTCTCTTCTGG	TGTTTCACTCAGTCGGACCTTT
ALKBH5	GGCTGCATCGTATCTCACGTA	AGCAGCATACCCACTGAGCAC
RUNX2	TCTTCCCAAAGCCAGAGCG	TGCCATTCGAGGTGGTCG
OPN	GAGGAGAAGGCGCATTACAG	AAACGTCTGCTTGTCTGCTG
BSP	TACGAACAAATAGGCAACGAGT	TTCGTCCTCATAAGCTCGGTAA
COL1	TGACTGGAAGAGCGGAGAGTA	GGGGTTTGGGCTGATGTACC

2.8. M6A-RT-PCR (MeRIP-qPCR)

After extraction with TRIzol, the total RNA was used for the m6A-IP-PCR (MeRIP-qPCR). Total RNA (1 μg) was taken out regraded as an input and was reverse transcribed to cDNA instantly. The remaining RNA (20 μg) was equally divided into RIP and IgG groups. The RNAs of the RIP and IgG groups were immunoprecipitated with 5 μg m6A antibody (Synaptic system, 202003, Germany) or anti-IgG (Cell Signaling Technology, 2729S, USA) in 500 μL IP buffer (150 mM NaCl, 0.1% NP-40, 10 mM Tris, pH 7.4, 100 U RNase inhibitor) at 4°C for 2 h. The liquid was then mixed with Pierce™ Protein A/G Magnetic Beads (Thermo Fisher Scientific, 88803, USA) and rotated for 2 h at 4°C after the beads were washed in 1 ml IP buffer twice. Afterward, the mixture was washed with 1 ml IP buffer 4 times and eluted twice with 50 μL elution buffer (5 mM Tris-HCl pH 7.5, 1 mM EDTA pH 8.0, 0.05% sodium dodecyl sulfate (SDS), 20 mg/ml Proteinase K) for 30 min. Then, the RNA was extracted with TRIzol and reverse transcribed to cDNA with random hexamers. cDNA (2 μL) from the RIP or IgG groups was used for qRT-PCR. Relative fold enrichment was calculated as $2^{-\Delta\Delta Ct}$. The primers for MeRIP-qPCR were as follows: Forward, 5' to 3', TGTACCACACAGGTCACGATT; reverse, 5' to 3', ATGAGGGGAGAAAATGCCAA.

2.9. RNA stability assays

To measure RNA stability, actinomycin D (Act-D; Sigma, A4262, USA) was added to the BMSCs at 5 μg/ml. After being incubated at 37°C for 0 h, 2 h, 4 h, and 6 h, the BMSCs were collected and RNA was extracted with TRIzol for qRT-PCR. GAPDH was used as an endogenous control.

2.10. Western blot analysis

The BMSCs were harvested using RIPA lysis buffer (Beyotime, P0013B, China) containing 1% protease and phosphatase inhibitor cocktail (100×) (Thermo Scientific, 78442, USA) and 1% phenylmethanesulfonyl fluoride (PMSF) (100 mM) (Beyotime, ST506, China) followed by centrifugation at 13,500 × g at 4°C for 15 min. The protein was mixed with SDS-PAGE protein loading buffer (Beyotime, P0286, China) and boiled at 99°C for 5 min. Equal amounts of protein lysates were subjected to SDS gel electrophoresis and transferred onto polyvinylidene fluoride (PVDF) membranes (Millipore, IPVH00010, USA). The membranes were then blocked in Tris-buffered saline Tween-20 containing 5% non-fat milk at room temperature for 1 h and incubated with a primary antibody at 4°C overnight. The membrane was incubated with a secondary antibody at room temperature for 1 h. Protein immunoreactivity was detected using LI-COR Odyssey Fluorescence Imaging System (LI-COR Biosciences, Lincoln, NE, USA) and the protein immunoreactive band intensity was measured using Image-Pro Plus 6.0. The antibodies used were as follows: METTL3 (1:1000; Proteintech, 15073-1-AP, USA), WTAP (1:6000; Proteintech, 60188-1-Ig, USA), ALKBH5 (1:6000; Proteintech, 16837-1-AP, USA), RUNX2 (1:1000; Cell Signaling Technology, 12556, USA), β-actin (1:6000; Proteintech, 66009-1-Ig, USA), anti-rabbit IgG (H+L) (DyLight™ 800 4X PEG Conjugate) (1:10,000; Cell Signaling Technology, 5151, USA), and anti-mouse IgG (H+L) (DyLight™ 800 4X PEG conjugate) (1:10,000; Cell Signaling Technology, 5257, USA).

2.11. Animal experiments

(1) Calvarial defect model

Eight-week-old SD rats were chosen for the animal experiments. All animal surgeries were performed under sterile conditions. The rats were anesthetized, and a 10 mm incision was made along the median line of the heads. Two calvarial defects with a diameter of 7 mm were made bilaterally using a circular bit. Then, the β-TCP scaffolds were implanted carefully into a random side, and the other side was used as a control. Subsequently, the skin was sutured and the wound was disinfected.

Animal experiments of this study were approved by the Ethics Committee of Shanghai Ninth People's Hospital, Shanghai JiaoTong University School of Medicine.

(2) Micro-computed tomography (micro-CT) analysis

Two months after the surgery, the SD rats were euthanized, and the skulls were collected. A micro-CT scanning

system (Bruker SkyScan 1176; Germany) was used to analyze the samples, which were scanned with a spot size of 10 μm, current of 250 μA, and maximum voltage of 40 kV. Then, the 3D images were reconstructed, and the bone volume fraction (BV/TV) and bone mineral density (BMD) were calculated using auxiliary software.

(3) Hematoxylin and eosin (H&E) staining and Masson staining

The skull samples were fixed with 4% paraformaldehyde and decalcified in 10% ethylenediaminetetraacetic acid. Then, the samples were embedded in paraffin and sectioned at a thickness of 5 μm. H&E staining and Masson's trichrome staining were performed as previously described[26].

(4) Immunohistochemistry

The sample sections were incubated with primary antibodies at 4°C overnight. The slides were then incubated with horseradish peroxidase (HRP)-conjugated secondary antibodies. Images were captured using a microscope and the numbers of positive cells were counted.

2.12. Statistical analysis

All results are expressed as mean ± standard deviation (SD). Error bars represent the SD. A two-tailed Student's *t*-test and one-way analysis of variance were used to analyze the difference between two groups and more than 2 groups, respectively; subsequently, Tukey's *post hoc* analysis was used to compare the differences between three or more groups. Statistical significance was set at $*P < 0.05$ and $**P < 0.01$.

3. Results

3.1. Characterization and biocompatibility of β-TCP extract

We prepared extract of β-TCP made of β-TCP powder. Size distribution analysis revealed a particle size smaller than 10,000 nm and mainly between 300 and 1000 nm (**Figure S1**). The zeta potential of β-TCP extract was −7.04 ± 0.69 mV (**Table S1**). Next, we diluted β-TCP extract into the ratios of 1/32, 1/64, and 1/128. The concentrations of Ca and P ions (Ctrl, 1/32, 1/64, and 1/128) were detected by ICP-AES, as shown in **Figure 1A**. The concentrations of Ca were 66.20 ± 1.53, 65.37 ± 0.81, 64.26 ± 0.97, and 65.79 ± 1.26 mg/L in Ctrl, 1/32, 1/64, and 1/128 dilutions, respectively, while the concentrations of P were 32.05 ± 1.64, 29.96 ± 0.65, 29.80 ± 0.96, and 30.99 ± 0.19 mg/L, respectively, which were consistent with a previous study and showed no significant difference in the concentrations of Ca and P[27].

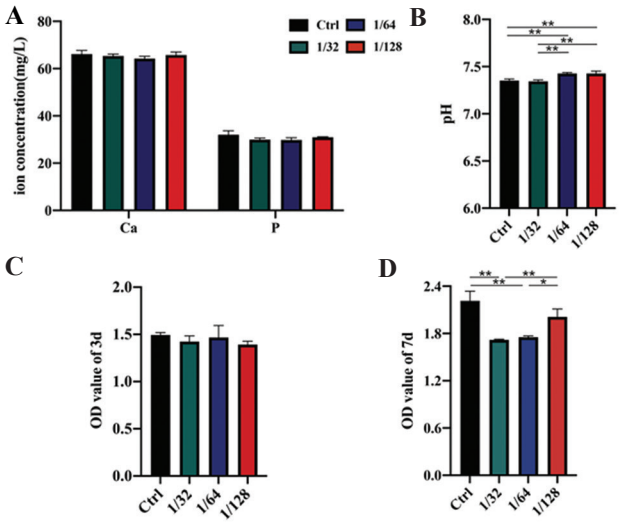

Figure 1. Characterization and biocompatibility of β-TCP extract. (A) Ion concentrations of Ca and P of α-MEM medium (Ctrl), α-MEM with 1/32 dilution of β-TCP extract (1/32), α-MEM with 1/64 dilution of β-TCP extract (1/64), and α-MEM with 1/128 dilution of β-TCP extract (1/128). (B) pH values of Ctrl, 1/32, 1/64, and 1/128 dilution groups. (C) OD values of BMSCs in Ctrl, 1/32, 1/64, and 1/128 dilution groups on day 3 by CCK-8. (D) OD values of BMSCs in Ctrl, 1/32, 1/64, and 1/128 groups on day 7 by CCK-8. $*P < 0.05$; $**P < 0.01$.

The pH values were 7.353 ± 0.012, 7.343 ± 0.012, 7.427 ± 0.009, and 7.427 ± 0.021, respectively (**Figure 1B**). The pH of the Ctrl and 1/32 dilution was significantly different from that of 1/64 and 1/128 dilutions ($P < 0.01$).

The cytotoxicity of the β-TCP extract was examined using the CCK-8 assay. It was found that BMSCs proliferated, and the cell numbers increased over time throughout the assay period. No significant difference was observed between the Ctrl and β-TCP extracts on day 3 after treatment, revealing no cytotoxicity of the β-TCP extract on day 3 (**Figure 1C**). On day 7 after treatment, however, the absorbance of 1/32 and 1/64 dilutions of β-TCP extract obviously decreased, showing a lower cell viability than the Ctrl and 1/128 dilution of β-TCP extract on day 7 (**Figure 1D**).

3.2. β-TCP promoted the osteogenic differentiation of BMSCs

We then tested the osteogenic differentiation of the BMSCs induced by β-TCP. As shown in **Figure 2A and B**, after induction for 7 days, all the groups treated with β-TCP extract showed approximately twice the ALP expression than those of the Ctrl. However, the expression among the three β-TCP groups showed no significant difference, suggesting that the β-TCP extract could induce osteogenic differentiation of BMSCs. We also examined the expression of bone formation-related genes. **Figures 2C-F** show that the levels of collagen type I

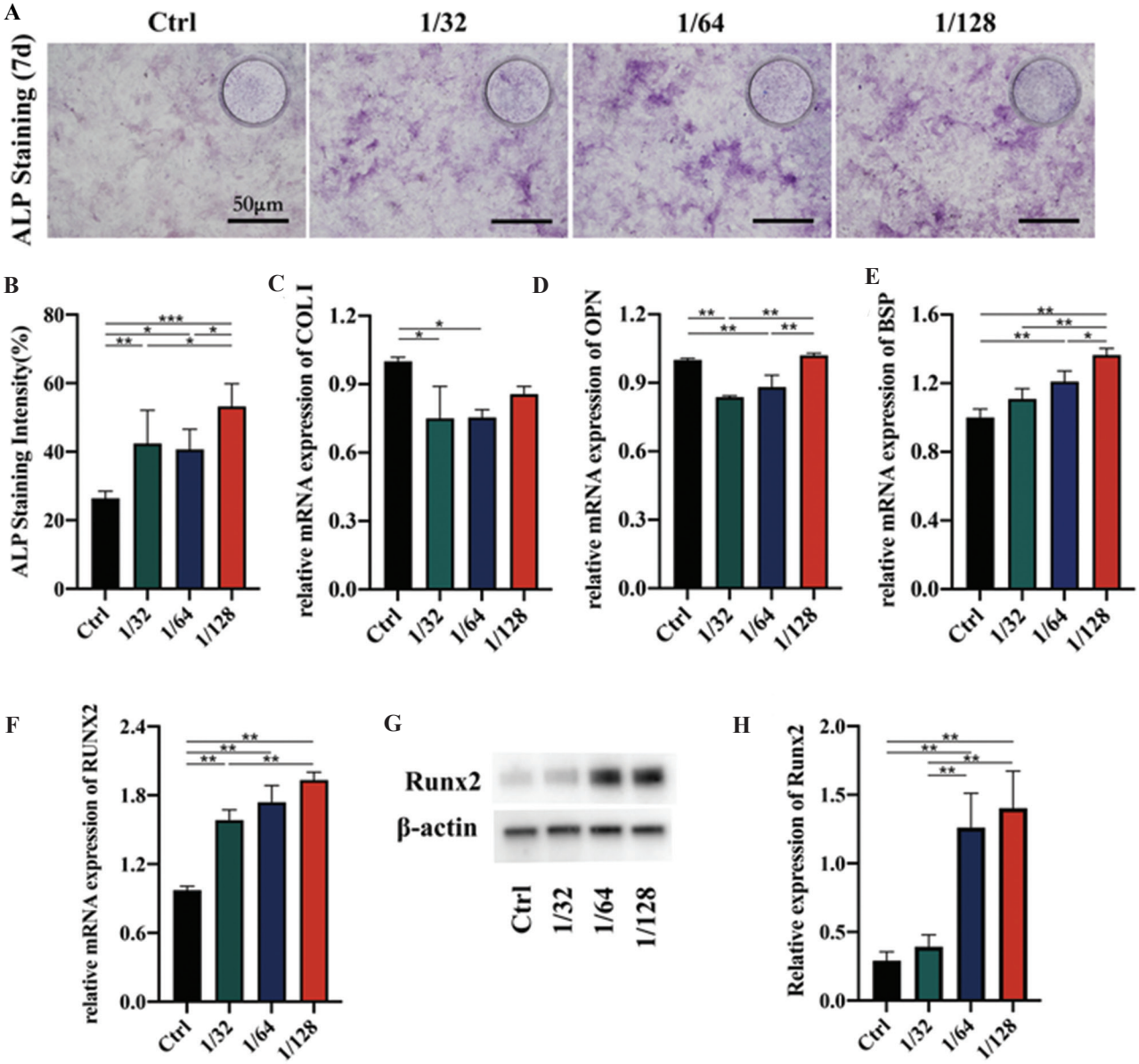

Figure 2. Osteogenesis effects of β-TCP on BMSCs. (A) ALP staining of BMSCs in Ctrl, 1/32, 1/64, and 1/128 groups. Top-right corner shows macroscopic pictures. Scale bars = 50 μm. (B) Quantitative results of (A). The mRNA expression levels of COL I (C), OPN (D), BSP (E), and RUNX2 (F) in Ctrl, 1/32, 1/64, and 1/128 dilution groups are illustrated in bar charts. The mRNA expression levels were determined by qRT-PCR. (G) The protein expression level of RUNX2 in Ctrl, 1/32, 1/64, and 1/128 dilution groups by Western blot. (H) The quantitative result of (G). *$P < 0.05$; **$P < 0.01$.

(COL I) and OPN, which represent late osteogenesis, in the β-TCP extract groups, were slightly lower than that of the Ctrl group, except for the 1/128 dilution of the β-TCP extract. Meanwhile, the levels of RUNX2 and BSP, which represent early osteogenesis, increased. Since RUNX2 was the key translation factor of osteogenesis, we further tested the expression of RUNX2 protein by Western blotting. The 1/64 and 1/128 dilutions of β-TCP extract showed higher expression of RUNX2 protein than the Ctrl (**Figure 2G and H**). These results demonstrated the excellent osteoinductivity of β-TCP. Considering the cytotoxicity and osteogenic differentiation assay results, we chose 1/128 dilutions of β-TCP extract for further experiments.

3.3. Expression level of m6A-related enzymes changed after β-TCP treatment

To study the effects of β-TCP on m6A-related enzymes such as "writers" and "erasers," we detected the mRNA and protein levels of several m6A-related enzymes. The results of the qRT-PCR analysis indicated that the

main m6A methyltransferases (METTL3, WTAP) and demethylases (ALKBH5) were significantly higher in the BMSCs after β-TCP induction at the mRNA level (**Figure 3A-C**). As determined by Western blotting, WTAP and ALKBH5 showed no statistically significant differences at protein level (**Figure 3D, F and G**). However, METTL3 expression was obviously increased (**Figure 3D and E**). All the results showed that β-TCP regulated the m6A-related enzymes, which might have an effect on the m6A level of osteogenesis-related genes.

3.4. RUNX2 showed higher m6A modification and the degradation of RUNX2 mRNA slowed down after β-TCP treatment

We further investigated the mechanism of RUNX2 increase after β-TCP treatment. First, we predicted the possible sites of RUNX2 that might be modified by m6A. As shown in **Figure 4A**, there were five sites that were likely to be modified by m6A with high possibility. We chose the 5279th site as the target site to design-specific primers (**Figure 4B**). It was found that the m6A level of RUNX2 in the BMSCs was significantly increased by β-TCP, which might lead to an increase in RUNX2 expression (**Figure 4C**). To explore the effects of the m6A level increase on the stability of RUNX2 mRNA, we used Act-D, an RNA polymerase II inhibitor, to detect the degradation of RUNX2 mRNA. The results showed that at 4 h and 6 h after the addition of Act-D, the degradation of RUNX2 mRNA treated with β-TCP significantly slowed down, that is, the half-life was prolonged (**Figure 4D**). All the data indicated that the m6A level of RUNX2 mRNA increased and the degradation of RUNX2 mRNA slowed down after the treatment with β-TCP.

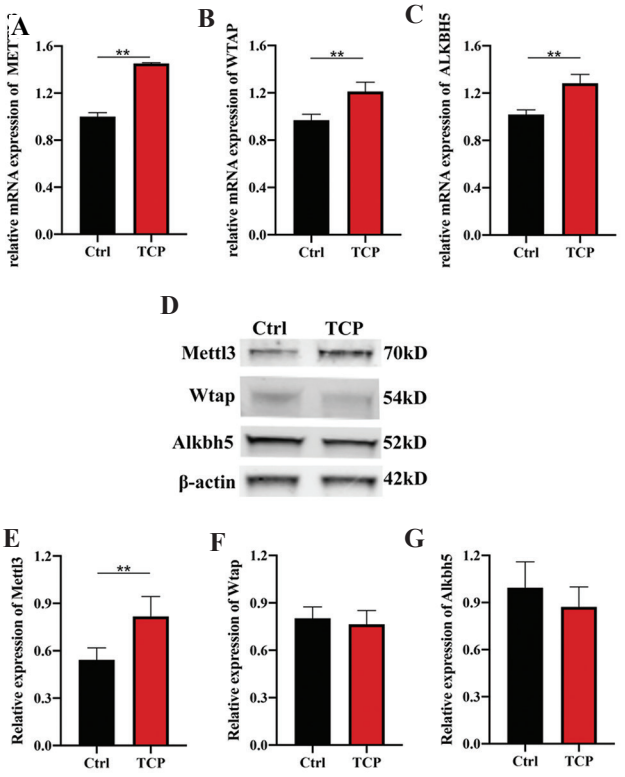

Figure 3. Expression level of m6A-related enzymes after β-TCP treatment. (A-C) The mRNA expression level of METTL3 (A), WTAP (B), and ALKBH5 (C) in the Ctrl and TCP (1/128 dilution) groups. The expression level was determined by qRT-PCR. (D) The protein expression level of METTL3, WTAP, and ALKBH5 in the Ctrl and TCP groups. (E-G) Quantitative results of (D). *$P < 0.05$; **$P < 0.01$.

3.5. β-TCP-induced osteogenesis in vivo

We further verified the effects of the β-TCP on osteogenesis in vivo. β-TCP scaffolds were manufactured by 3D printer (**Figure 5A**), and the diameter of which was about 7 mm each (**Figure 5B**). The scaffolds were made porous so that they were beneficial for adhesion of BMSCs. The surface microstructure of β-TCP scaffolds was demonstrated by SEM. Microscopically, the surface of β-TCP scaffolds was also porous and rough, although some particles were sintered together (**Figure 5C**). To embed β-TCP into bone defect sites of rat cranial defect models (**Figure 5D**), we manufactured β-TCP scaffolds using 3D printing technology. Eight weeks after model construction, we sacrificed the rats to obtain the skull samples for micro-CT analyses. It was shown that some new bone was formed inside and outside the cranial defect (yellow section) (**Figure 5E**). Next, bone volume fraction (BV/TV) and BMD were evaluated to assess new bone formation. As shown in **Figure 5F** and **5G**, BV/TV and BMD in the β-TCP group increased approximately 2-fold compared to that in the Ctrl group. The above findings indicated that β-TCP-induced osteogenesis effectively and significantly. Next, H&E and Masson's trichrome staining were performed to analyze the proportion of osteogenic tissue. H&E staining showed that the bone defect site was filled with soft tissue in the Ctrl group but was surrounded by newly formed bone in the β-TCP group (**Figure 5H**). Consistent with the H&E staining, the Masson's trichrome staining showed that more new bone was present in the β-TCP group (**Figure 5I**). All the above data indicated that TCP induced new bone formation.

3.6. β-TCP increased the expression of METTL3 in vivo

Furthermore, we investigated the expression levels of a series of osteogenic factors and m6A-related enzymes in vivo. RUNX2, OCN, and OPN are the most common proteins involved in osteogenesis[3,26]. After β-TCP treatment, the expression levels of RUNX2, OCN, and OPN were significantly increased, indicating the osteoinductivity of TCP in vivo (**Figure 6A-D**).

A

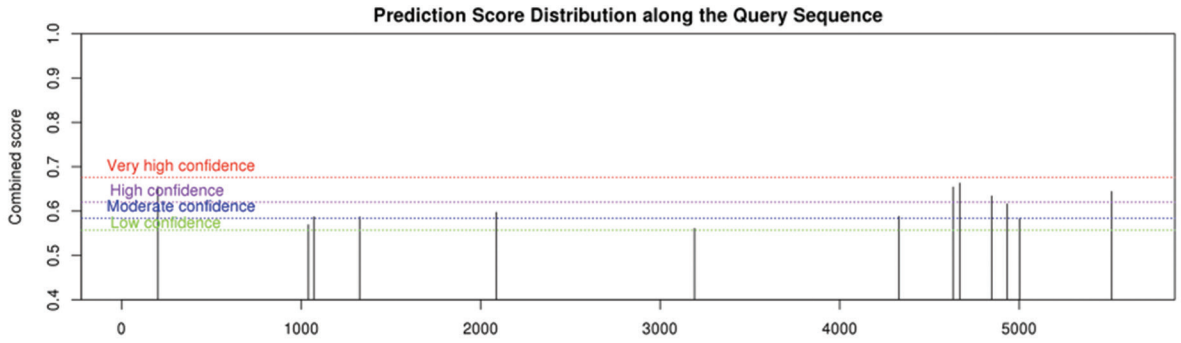

B

4094	UUUAC AAUAC AGUUA UUAAG GGACU AGAGG GGAUG CCUUA GUGCC	N/A	N/A	0.683	0.730	0.440	0.588	m^6A site (Moderate confidence)
4396	AAUGU CUUAA UACUC UCCUG GGACU GUUUU CGUGU ACAAA CUUCC	N/A	N/A	0.714	0.837	0.548	0.654	m^6A site (High confidence)
4433	AAACU UCCCU GGGCU UAGAU GGACA UGGUU CUCGA AGGAG CACAA	N/A	N/A	0.663	0.559	0.675	0.663	m^6A site (High confidence)
4611	GCACC CAGCC CAUAA UAGAA AGACU UACCA GAUUU AACUA GUUGG	N/A	N/A	0.732	0.551	0.511	0.634	m^6A site (High confidence)
4697	CAACA UCUCC ACAUC AUUAG AGACU GUCCA CAGUA GGUUC AGAAG	N/A	N/A	0.739	0.644	0.445	0.616	m^6A site (Moderate confidence)
4766	CUUGC UCCAA GGAAA GGCAC UGACU GACCU AGUUU UAGAG AACAG	N/A	N/A	0.612	0.475	0.557	0.583	m^6A site (Low confidence)
5279	GUUUA CUCUG AACUU CAAAG GGACU AUUUG UAUUG UAUGU UGCAA	N/A	N/A	0.734	0.647	0.521	0.644	m^6A site (High confidence)

C

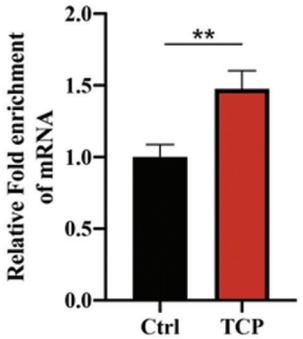

D

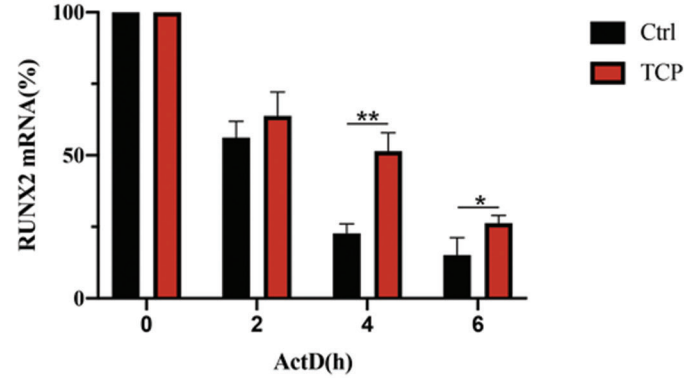

Figure 4. m6A level of RUNX2 mRNA and the stability of RUNX2 mRNA after TCP treatment. (A) Possible sites with m6A modification of RUNX2 mRNA. (B) Sequences of possible sites with m6A modification. (C) M6A level of RUNX2 mRNA in BMSCs in the Ctrl and TCP groups. (D) The decay of RUNX2 mRNA after TCP treatment at 0, 2, 4, and 6 h. * $P < 0.05$; ** $P < 0.01$.

Moreover, the expression levels of m6A-related enzymes were detected by immunohistochemistry. Identical to the in vitro results, the expression level of METTL3 on the TCP group was approximately 1.5-fold higher than that of the Ctrl group (**Figure 6E** and **F**). However, the expression levels of WTAP and ALKBH5 were not significantly different between the two groups, suggesting that METTL3 played a key role in the process of osteogenesis induced by β-TCP (**Figure 6E, G, H**). All the results indicated that β-TCP increased osteogenic proteins in calvarial defect models, and METTL3 other than WTAP or ALKBH5 promoted the osteogenesis.

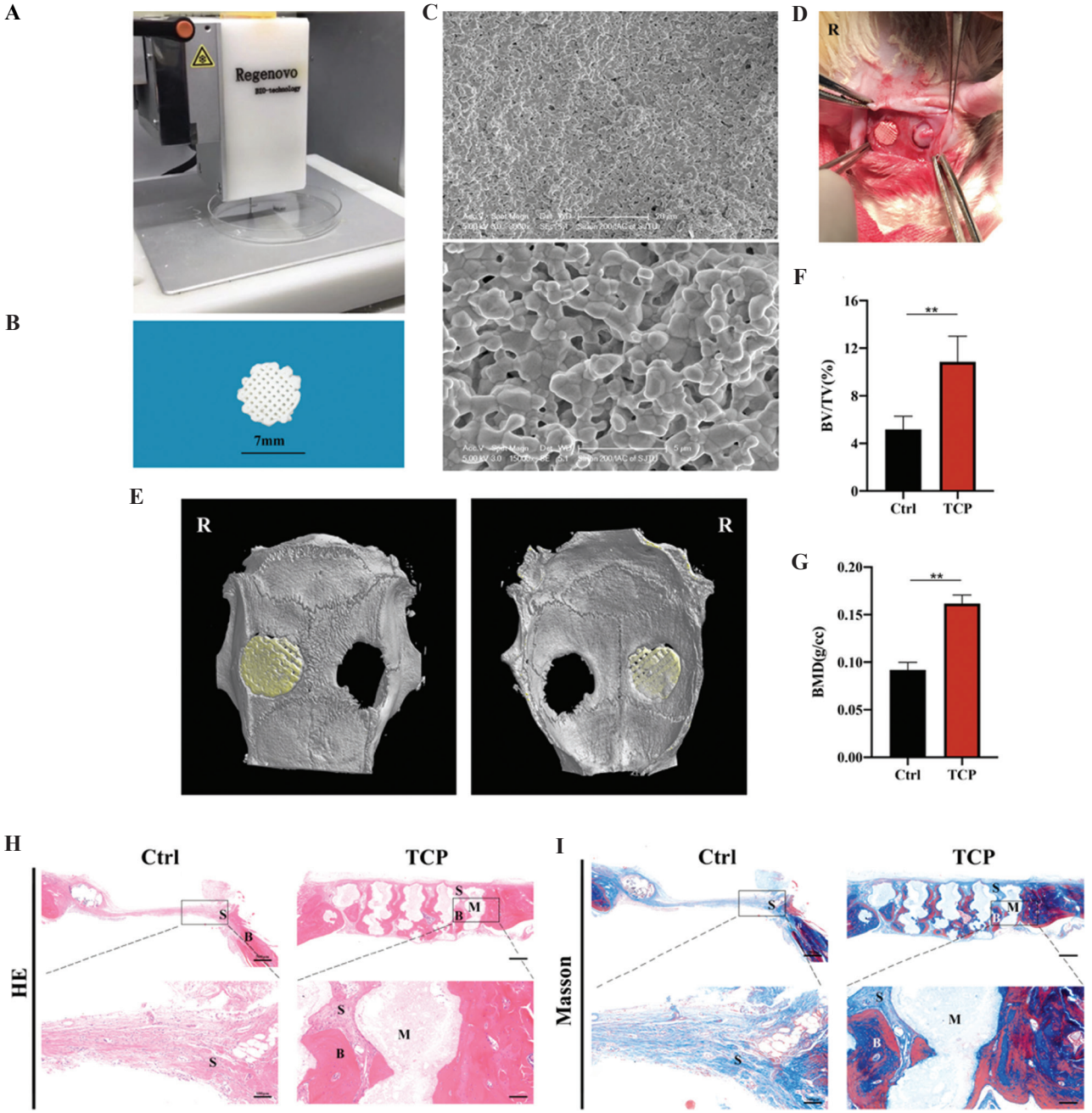

Figure 5. Osteogenesis effects of β-TCP scaffolds in vivo. (A) β-TCP scaffolds were made. (B) The appearance of β-TCP scaffolds with the diameter of around 7 mm. (C) SEM images of the surface microstructure of β-TCP scaffolds. (D) Rat cranial defect models were constructed. (E) 3D reconstruction of micro-CT images. (F) Quantitative analysis of BV/TV of micro-CT images. (G) Quantitative analysis of BMD of micro-CT images. (H) H&E staining of skull samples. Scale bars = 500 μm, 100 μm, respectively. (I) Masson staining of skull samples. Scale bars = 500 μm, 100 μm, respectively. S: Soft tissue; B: Bone; M: Material. *$P < 0.05$; **$P < 0.01$

4. Discussion

Collectively, our study demonstrated that β-TCP scaffolds made by 3D printing technology could induce osteogenic differentiation of BMSCs in vitro. Meanwhile, BMSCs stimulated by β-TCP extract had significantly higher expression of METTL3 in the β-TCP group than in the control group, which affected m6A modification of RNA in BMSCs. Mechanistically, the m6A level of RUNX2 in BMSCs increased after β-TCP treatment, leading to improved stability of RUNX2 mRNA and retardation of decay of RUNX2 mRNA, which indirectly facilitates an increase of RUNX2 mRNA and protein (**Figure 7**). According to the animal experiments, we found that β-TCP promoted new bone formation and increased

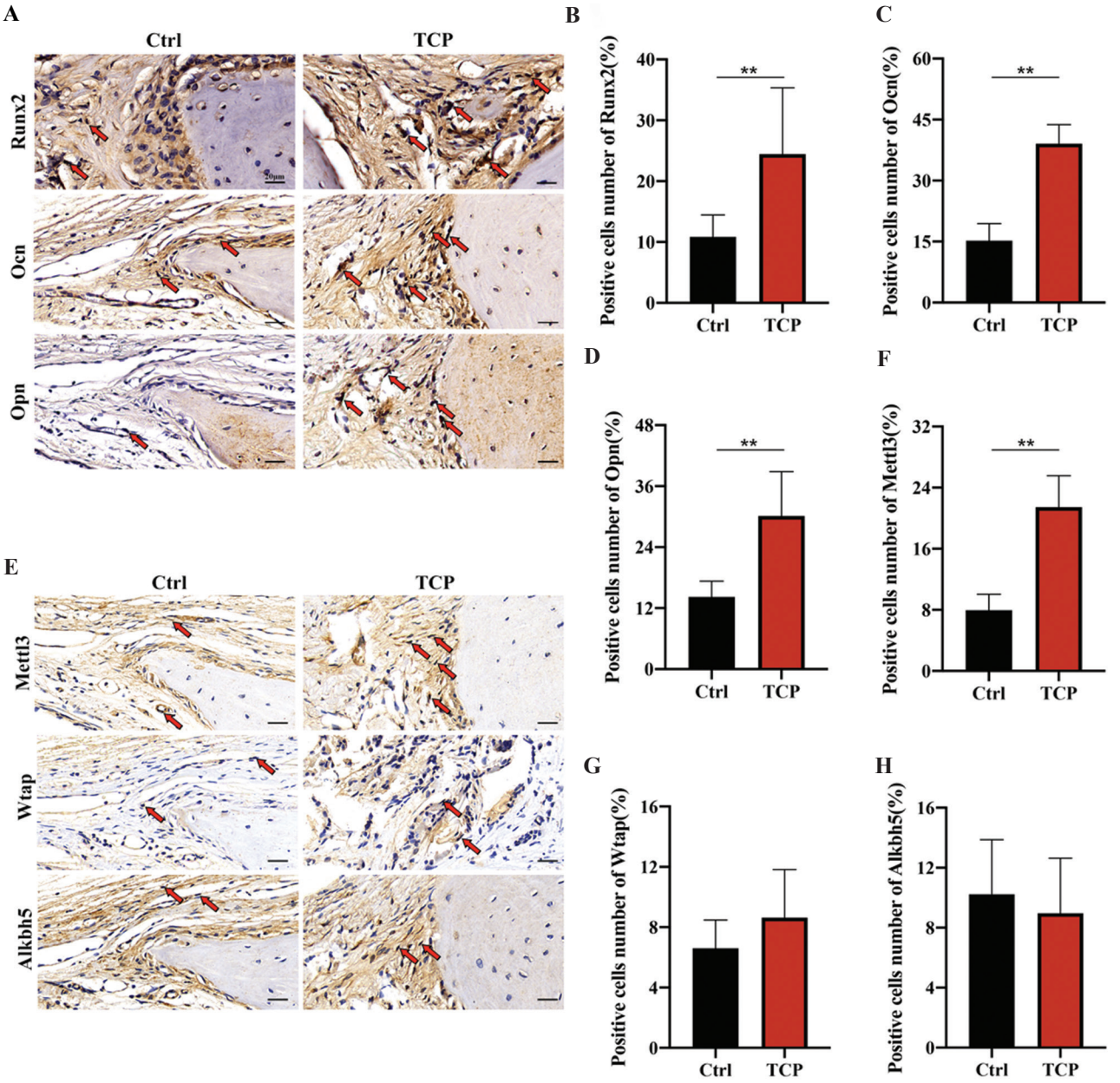

Figure 6. Immunohistochemistry analysis of osteogenic factors and m6A-related enzymes. (A) Immunohistochemistry analysis of Runx2, Ocn, and Opn in the Ctrl and TCP groups. Arrows represented positive cells. Scale bars = 20 μm. (B-D) Quantitative results of Runx2 (B), Ocn (C), and Opn (D). (E) Immunohistochemistry analysis of METTL3, WTAP, and ALKBH5 in the Ctrl and TCP groups. Arrows represented positive cells. Scale bars = 20 μm. (F-H) Quantitative results of METTL3 (F), WTAP (G), and ALKBH5 (H). *$P < 0.05$; **$P < 0.01$.

METTL3 expression. These results suggested that β-TCP could promote the osteogenic differentiation of BMSCs by increasing the m6A modification of RUNX2.

Bones have numerous key roles in the human body, such as acting as a framework to support the body, protecting internal organs from injury, enabling body movements, producing blood cells, and maintaining calcium homeostasis[28]. Bone tumors, injury, and other bone diseases are likely to lead to bone defects. For a long time, bone defects have been a serious orthopedic disease which downgrades the quality of life of patients[29]. In view of the limited bone repair capacity of autologous BMSCs, it is necessary to use natural or synthetic bone as a replacement in bone grafting[30]. In general, autogenous bone grafts are the gold standard material for bone substitutes[31]. Nevertheless, the inadequacies of allograft bone and finite autogenous bone resources impose restrictions on their clinical application[32].

The development of bone tissue engineering provides a new prospect for treating bone defects. The most important point is choosing feasible materials, which requires a balance between new bone formation and material

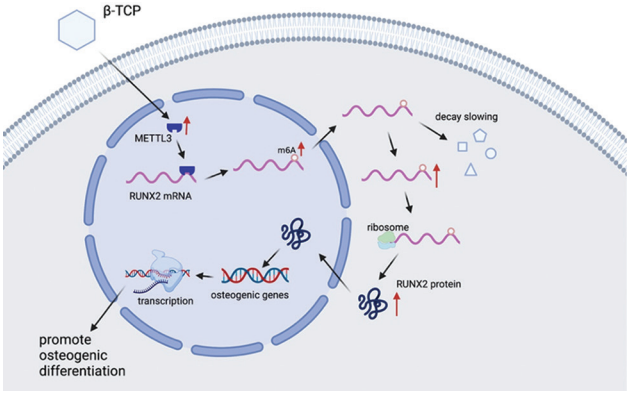

Figure 7. The mechanism of β-TCP contributing osteogenesis of BMSCs. β-TCP increases the expression of METTL3, which leads to an increase of m6A level of RUNX2 in BMSCs. The upregulation of m6A level helps stabilize the RUNX2 mRNA, which indirectly facilitates the increase of RUNX2 mRNA. As a consequence, more RUNX2 protein promotes the transcription of other osteogenic factors, launching the osteogenic differentiation of BMSCs. The illustration was made using BioRender (https://biorender.com/).

degradation. Being one of the most crucial components of the bone[33], HA was one of the materials studied in the early stage for its bone repair potential[34,35]. HA has been used in clinical treatment because of its good cytocompatibility[36]. Composites consisting of HA, such as polylysine-modified coral HA, collagen-HA-based scaffolds, and chitosan/curdlan/HA biomaterials, have been proven to improve osteogenesis[37,38]. TCP, which is composed of phosphate radicals and calcium ions in aqueous solution, is a new bone substitute for bone regeneration. It is known that calcium and phosphorus are the two fundamental elements of bones. Therefore, these two elements of β-TCP promote bone regeneration. Herein, we detected the release of calcium and phosphorus, which was also reported in a previous study[27]. No significant difference existing among the four groups was possibly linked to the precipitation of calcium phosphate. Since β-TCP extract showed alkalescence, which was identical to pH values of body fluids, it had good biocompatibility. Numerous studies have demonstrated the cytocompatibility and osteoinductivity of TCP and its composites[39]. Herein, our results suggested that β-TCP extract showed low cytotoxicity, which disappeared after the extract was diluted (in 1/128 dilution).

At the same time, the BMSCs stimulated by β-TCP tended to undergo osteogenic differentiation relative to the cells received no treatment; this was confirmed by ALP staining and determination of mRNA and protein expression of osteogenic factors. These results were consistent with those of the previous studies[40]. Among the osteogenic factors, RUNX2 has been proven to be a key transcriptional factor that triggers the activation of other factors and promotes osteogenic differentiation of BMSCs. Thus, RUNX2 was regarded as a target gene in this study.

The mechanism by which β-TCP contributes to osteogenesis is not well understood. To begin with investigating the mechanism, we note that the m6A modification shows strong association with osteogenesis, and METTL3 affects the osteogenic differentiation of BMSCs through the PI3K-Akt signaling pathway and the expression level of VEGF[41]. In C3H10T1/2 cells, FTO and p-AMPK form a positive feedback loop, stimulating endoplasmic reticulum (ER) stress and inducing osteogenic differentiation[42]. In view of the above, we investigated the mechanism by which β-TCP contributed to osteogenesis in terms of m6A modification. It was found that mRNA and protein levels of METTL3 both increased after β-TCP treatment, hinting at the significance of METTL3 in the process of osteogenesis induced by β-TCP. M6A RNA methylation is the most prevalent post-transcriptional modification in mammals[43]. Usually, m6A modification is regulated by methyltransferases and demethylases, and then is identified by "readers"[44]. Recently, a growing number of studies have focused on the effects of m6A modifications on osteogenesis. Zhang *et al*. found that METTL3 knockdown suppressed osteoblast differentiation and Smad-dependent signaling by stabilizing Smad7 and Smurf1 mRNA transcripts in a YTHDF2-dependent manner[45]. METTL3 is the most important methyltransferases. In our study, METTL3 also showed increase while the other m6A-related enzymes did not.

There are many ways that m6A modification can regulate mRNA in cells, depending on different m6A binding proteins. Recent studies have reported new findings on the m6A post-transcriptional modification in the regulation of RNA transcription[46], splicing[47], processing events[48], RNA stability[49], and translation[50]. Among these, cytoplasmic mRNA stability and reduction in mRNA stability are crucial for cell activities. Thus, we studied the mechanism of β-TCP osteoinductivity in detail. The results showed that β-TCP increased the m6A level of RUNX2 after β-TCP treatment by MeRIP-qPCR. Simultaneously, the m6A level increase also resulted in improved stability of RUNX2 mRNA induced by β-TCP, and increased the mRNA and protein expression of RUNX2, contributing to osteogenesis of BMSCs.

Finally, we verified the osteogenesis of β-TCP through animal experiments. The calvarial defect model is the most commonly used model for bone defects. The micro-CT results suggested that more new bone was formed after β-TCP induction. Likewise, the expression of RUNX2, OCN, and OPN showed similar tendency to those of the micro-CT. Besides, METTL3 expression level also increased in the β-TCP embedded side, implying that METTL3 exerted a vital influence on the osteogenesis process. We also performed immunohistochemistry analysis of m6A-related enzymes to study the effects

of β-TCP in vivo, which shed light on the mechanism of osteoinductivity of β-TCP from the perspective of epigenetic modifications.

5. Conclusions

In this study, we investigated the effect of β-TCP on osteogenic differentiation of BMSCs. The underlying mechanism is that β-TCP increases the expression of METTL3, leading to a higher m6A level of RUNX2. The rise of m6A level results in the retardation of decay and enhanced stability of RUNX2 mRNA, causing an increase of RUNX2 mRNA and protein levels. As a result, RUNX2 triggers the transcription of other osteogenic factors and promotes osteogenic differentiation of BMSCs.

Funding

This work was supported by the National Key Research and Development Program of China (2017YFC110390), National Natural Science Foundation of China (82172402), Funds of the Clinical Research Plan of SHDC (16CR3099B), and National Natural Science Foundation of China (82072412).

Conflicts of interest

All the authors declare no conflicts of interest.

Authors' contributions

Y.G. and J.W. designed the study. X.J. and X.S. performed the experiments. X.J. and W.L. interpreted data and wrote the manuscript. W.C., Y.Z., and Y.L. helped analyze the data. Z.W., X.Z., J.M., C.X., and K.D. provided experimental assistance. Y.G. supervised the project. All authors read and approved the manuscript.

References

1. Wang Z, Guo Z, Bai H, *et al.*, 2013, Clinical Evaluation of β-TCP in the Treatment of Lacunar Bone Defects: A Prospective, Randomized Controlled Study. *Mater Sci Eng C*, 33:1894–9. https://doi.org/10.1016/j.msec.2012.12.041
2. Seebach C, Henrich D, Kähling C, *et al.*, 2010, Endothelial Progenitor Cells and Mesenchymal Stem Cells Seeded onto β-TCP Granules Enhance Early Vascularization and Bone Healing in a Critical-Sized Bone Defect in Rats. *Tissue Eng Part A*, 16:1961–70. https://doi.org/10.1089/ten.tea.2009.0715
3. Chu W, Zhuang Y, Gan Y, *et al.*, 2019, Comparison and Characterization of Enriched Mesenchymal Stem Cells Obtained by the Repeated Filtration of Autologous Bone Marrow Through Porous Biomaterials. *J Transl Med*, 17:377. https://doi.org/10.1186/s12967-019-02131-y
4. Chu W, Gan Y, Zhuang Y, *et al.*, 2018, Mesenchymal Stem Cells and Porous β-tricalcium Phosphate Composites Prepared through Stem Cell Screen-enrich-combine (Biomaterials) Circulating System for the Repair of Critical Size Bone Defects in Goat Tibia. *Stem Cell Res Ther*, 9:157. https://doi.org/10.1186/s13287-018-0906-1
5. Chu W, Wang X, Gan Y, *et al.*, 2019, Screen-enrich-combine Circulating System to Prepare MSC/β-TCP for Bone Repair in Fractures with Depressed Tibial Plateau. *Regener Med*, 14:555–69. https://doi.org/10.2217/rme-2018-0047
6. Wang X, Chu W, Zhuang Y, *et al.*, 2019, Bone Mesenchymal Stem Cell-Enriched β-Tricalcium Phosphate Scaffold Processed by the Screen-Enrich-Combine Circulating System Promotes Regeneration of Diaphyseal Bone Non-Union. *Cell Transplant*, 28:212–23. https://doi.org/10.1177/0963689718818096
7. Masaoka T, Yoshii T, Yuasa M, *et al.*, 2016, Bone Defect Regeneration by a Combination of a β-Tricalcium Phosphate Scaffold and Bone Marrow Stromal Cells in a Non-Human Primate Model. *Open Biomed Eng J*, 10: 2-11. https://doi.org/10.2174/1874120701610010002
8. Barradas AM, Monticone V, Hulsman M, *et al.*, 2013, Molecular Mechanisms of Biomaterial-driven Osteogenic Differentiation in Human Mesenchymal Stromal Cells. *Integr Biol*, 5:920–31. https://doi.org/10.1039/c3ib40027a
9. Liu J, Zhao L, Ni L, *et al.*, 2015, The Effect of Synthetic α-tricalcium Phosphate on Osteogenic Differentiation of Rat Bone Mesenchymal Stem Cells. *Am J Transl Res*, 7:1588–601.
10. Rittipakorn P, Thuaksuban N, Mai-Ngam K, *et al.*, 2021, Bioactivity of a Novel Polycaprolactone-Hydroxyapatite Scaffold Used as a Carrier of Low Dose BMP-2: An In Vitro Study. *Polymers* (*Basel*), 13:466. https://doi.org/10.3390/polym13030466
11. Hesse E, Saito H, Kiviranta R, *et al.*, 2010, Zfp521 Controls Bone Mass by HDAC3-dependent Attenuation of Runx2 Activity. *J Cell Biol*, 191:1271–83. https://doi.org/10.1083/jcb.201009107
12. Liu JC, Lengner CJ, Gaur T, *et al.*, 2011, Runx2 Protein Expression Utilizes the Runx2 P1 Promoter to Establish Osteoprogenitor Cell Number for Normal Bone Formation. *J Biol Chem*, 286:30057–70. https://doi.org/10.1074/jbc.M111.241505
13. Kronenberg HM, 2004, Twist Genes Regulate Runx2 and Bone Formation. *Dev Cell*, 6:317–8. https://doi.org/10.1016/S1534-5807(04)00069-3

14. Yan G, Yuan Y, He M, *et al.*, 2020, m6A Methylation of Precursor-miR-320/RUNX2 Controls Osteogenic Potential of Bone Marrow-Derived Mesenchymal Stem Cells. *Mol Ther Nucleic Acids*, 19:421–36. https://doi.org/10.1016/j.omtn.2019.12.001
15. Chen J, Tian Y, Zhang Q, *et al.*, 2021, Novel Insights into the Role of N6-Methyladenosine RNA Modification in Bone Pathophysiology. *Stem Cells Dev*, 30:17–28. https://doi.org/10.1089/scd.2020.0157
16. Lee M, Kim B, Kim VN, 2014, Emerging Roles of RNA Modification: m 6 A and U-Tail. *Cell*, 158:980–7. https://doi.org/10.1016/j.cell.2014.08.005
17. Zhao BS, Roundtree IA, He C, 2017, Post-transcriptional Gene Regulation by mRNA Modifications. *Nat Rev Mol Cell Biol*, 18:31–42. https://doi.org/10.1038/nrm.2016.132
18. He C, 2010, Grand Challenge Commentary: RNA epigenetics? *Nat Chem Biol*, 6:863–65. https://doi.org/10.1038/nchembio.482
19. Yang Y, Hsu PJ, Chen YS, *et al.*, 2018, Dynamic Transcriptomic m6A Decoration: Writers, Erasers, Readers and Functions in RNA Metabolism. *Cell Res*, 28:616–24. https://doi.org/10.1038/s41422-018-0040-8
20. Wu Y, Xie L, Wang M, *et al.*, 2018, Mettl3-mediated m6A RNA Methylation regulates the fate of bone marrow mesenchymal stem cells and osteoporosis. *Nat Commun*, 9:4772. https://doi.org/10.1038/s41467-018-06898-4
21. Yu J, Shen L, Liu Y, *et al.*, 2020, The m6A Methyltransferase METTL3 Cooperates with Demethylase ALKBH5 to Regulate Osteogenic Differentiation through NF-κB Signaling. *Mol Cell Biochem*, 463:203–10. https://doi.org/10.1007/s11010-019-03641-5
22. Liu Y, Gu C, Li X, *et al.*, 2021, Involvement of METTL3/m6Adenosine and TGFβ/Smad3 Signaling on Tenon's Fibroblasts and in a Rabbit Model of Glaucoma Surgery. *J Mol Histol*, 52:1129–44. https://doi.org/10.1007/s10735-021-10028-8
23. Liu L, Yu F, Li L, *et al.*, 2021, Bone Marrow Stromal Cells Stimulated by Strontium-substituted Calcium Silicate Ceramics: Release of Exosomal miR-146a Regulates Osteogenesis and Angiogenesis. *Acta Biomater*, 119:444–57. https://doi.org/10.1016/j.actbio.2020.10.038
24. Zhou P, Xia D, Ni Z, *et al.*, 2021, Calcium Silicate Bioactive Ceramics Induce Osteogenesis through Oncostatin M. *Bioact Mater*, 6:810–22. https://doi.org/10.1016/j.bioactmat.2020.09.018
25. Huang Y, Jin X, Zhang X, *et al.*, 2009, *In Vitro* and *In Vivo* Evaluation of Akermanite Bioceramics for Bone Regeneration. *Biomaterials*, 30:5041–8. https://doi.org/10.1016/j.biomaterials.2009.05.077
26. Sun X, Ma Z, Zhao X, *et al.*, 2021, Three-dimensional Bioprinting of Multicell-laden Scaffolds Containing Bone Morphogenic Protein-4 for Promoting M2 Macrophage Polarization and Accelerating Bone Defect Repair in Diabetes Mellitus. *Bioact Mater*, 6:757–69. https://doi.org/10.1016/j.bioactmat.2020.08.030
27. Zheng M, Weng M, Zhang X, *et al.*, 2021, Beta-tricalcium Phosphate Promotes Osteogenic Differentiation of Bone Marrow-derived Mesenchymal Stem Cells through Macrophages. *Biomed Mater*, 16:025005. https://doi.org/10.1088/1748-605X/abdbdc
28. El-Rashidy AA, Roether JA, Harhaus L, *et al.*, 2017, Regenerating Bone with Bioactive Glass Scaffolds: A Review of *In Vivo* Studies in Bone Defect Models. *Acta Biomater*, 62:1–28. https://doi.org/10.1016/j.actbio.2017.08.030
29. Wu D, Wang Z, Wang J, *et al.*, 2018, Development of a Micro-tissue-mediated Injectable Bone Tissue Engineering Strategy for Large Segmental Bone Defect Treatment. *Stem Cell Res Ther*, 9:331. https://doi.org/10.1186/s13287-018-1064-1
30. Stevens MM, 2008, Biomaterials for Bone Tissue Engineering. *Mater Today*, 11:18–25. https://doi.org/10.1016/S1369-7021(08)70086-5
31. Baldwin P, Li DJ, Auston DA, *et al.*, 2019, Autograft, Allograft, and Bone Graft Substitutes: Clinical Evidence and Indications for Use in the Setting of Orthopaedic Trauma Surgery. *J Orthop Trauma*, 33:203–13. https://doi.org/10.1097/BOT.0000000000001420
32. Prakash J, Prema D, Venkataprasanna KS, *et al.*, 2020, Nanocomposite Chitosan Film Containing Graphene Oxide/Hydroxyapatite/Gold for Bone Tissue Engineering. *Int J Biol Macromol*, 154:62–71. https://doi.org/10.1016/j.ijbiomac.2020.03.095
33. Kaushik N, Nguyen LN, Kim JH, *et al.*, 2020, Strategies for Using Polydopamine to Induce Biomineralization of Hydroxyapatite on Implant Materials for Bone Tissue Engineering. *Int J Mol Sci*, 21:E6544. https://doi.org/10.3390/ijms21186544
34. Take Y, Mae T, Yoneda M, *et al.*, 2020, On-lay Grafting of a Calcium Hydroxyapatite Bone Substitute: A Preliminary Animal Experimental Study. *J Orthop Sci*, 25:1101–6. https://doi.org/10.1016/j.jos.2019.12.012

35. Sathiyavimal S, Vasantharaj S, Oscar FL, *et al.*, 2019, Biosynthesis and Characterization of Hydroxyapatite and its Composite (Hydroxyapatite-gelatin-chitosan-fibrin-bone Ash) for Bone Tissue Engineering Applications. *Int J Biol Macromol*, 129:844–52. https://doi.org/10.1016/j.ijbiomac.2019.02.058

36. Beuriat PA, Lohkamp LN, Szathmari A, *et al*., 2019, Repair of Cranial Bone Defects in Children Using Synthetic Hydroxyapatite Cranioplasty (CustomBone). *World Neurosurg*, 129:e104–13. https://doi.org/10.1016/j.wneu.2019.05.052

37. Zhang H, Zhou Y, Yu N, *et al.*, 2019, Construction of Vascularized Tissue-engineered Bone with Polylysine-modified Coral Hydroxyapatite and a Double Cell-sheet Complex to Repair a Large Radius Bone Defect in Rabbits. *Acta Biomater*, 91:82–98. https://doi.org/10.1016/j.actbio.2019.04.024

38. Przekora A, Kazimierczak P, Wojcik M, 2021, *Ex Vivo* Determination of Chitosan/Curdlan/Hydroxyapatite Biomaterial Osseointegration with the Use of Human Trabecular Bone Explant: New Method for Biocompatibility Testing of Bone Implants Reducing Animal Tests. *Mater Sci Eng C Mater Biol Appl*, 119:111612. https://doi.org/10.1016/j.msec.2020.111612

39. Putri TS, Hayashi K, Ishikawa K, 2020, Bone Regeneration Using β-tricalcium Phosphate (β-TCP) block with Interconnected Pores Made by Setting Reaction of β-TCP Granules. *J Biomed Mater Res A*, 108:625–32. https://doi.org/10.1002/jbm.a.36842

40. Zhang D, Gao P, Li Q, *et al.*, Engineering Biomimetic Periosteum with β-TCP Scaffolds to Promote Bone Formation in Calvarial Defects of Rats. *Stem Cell Res Ther*, 8:134. https://doi.org/10.1186/s13287-017-0592-4

41. Tian C, Huang Y, Li Q, *et al.*, 2019, Mettl3 Regulates Osteogenic Differentiation and Alternative Splicing of Vegfa in Bone Marrow Mesenchymal Stem Cells. *Int J Mol Sci*, 20:551. https://doi.org/10.3390/ijms20030551

42. Son HE, Min HY, Kim EJ, *et al.*, 2020, Fat Mass and Obesity-Associated (FTO) Stimulates Osteogenic Differentiation of C3H10T1/2 Cells by Inducing Mild Endoplasmic Reticulum Stress via a Positive Feedback Loop with p-AMPK. *Mol Cells*, 43:58–65.

43. Zhang C, Chen Y, Sun B, *et al.*, 2017, m6A Modulates Haematopoietic Stem and Progenitor Cell Specification. *Nature*, 549:273–6. https://doi.org/10.1038/nature23883

44. Zhang B, Wu Q, Li B, *et al.*, 2020, m6A Regulator-Mediated Methylation Modification Patterns and Tumor Microenvironment Infiltration Characterization in Gastric Cancer. *Mol Cancer*, 19:53. https://doi.org/10.1186/s12943-020-01170-0

45. Zhang Y, Gu X, Li D, *et al.*, 2019, METTL3 Regulates Osteoblast Differentiation and Inflammatory Response via Smad Signaling and MAPK Signaling. *Int J Mol Sci*, 21:199. https://doi.org/10.3390/ijms21010199

46. Barbieri I, Tzelepis K, Pandolfini L, *et al.*, 2017, Promoter-bound METTL3 Maintains Myeloid Leukaemia by m6A-dependent Translation Control. *Nature*, 552:126–31. https://doi.org/10.1038/nature24678

47. Dominissini D, Moshitch-Moshkovitz S, Schwartz S, *et al.*, 2012, Topology of the Human and Mouse m6A RNA Methylomes Revealed by m6A-seq. *Nature*, 485:201–6. https://doi.org/10.1038/nature11112

48. Bartosovic M, Molares HC, Gregorova P, *et al.*, 2017, N6-methyladenosine Demethylase FTO Targets pre-mRNAs and Regulates Alternative Splicing and 3'-end Processing. *Nucleic Acids Res*, 45:11356–70. https://doi.org/10.1093/nar/gkx778

49. Geula S, Moshitch-Moshkovitz S, Dominissini D, *et al.*, 2015, Stem Cells. m6A mRNA Methylation Facilitates Resolution of Naïve Pluripotency toward Differentiation. *Science*, 347:1002–6. https://doi.org/10.1126/science.1261417

50. Kennedy EM, Bogerd HP, Kornepati AV, *et al.*, 2017, Posttranscriptional m6A Editing of HIV-1 mRNAs Enhances Viral Gene Expression. *Cell Host Microbe*, 22:830. https://doi.org/10.1016/j.chom.2017.11.010

Publisher's note